

THE VARIATION OF MAGNESIUM DEPLETION WITH LINE OF SIGHT CONDITIONS

Adam G. Jensen and Theodore P. Snow

Center for Astrophysics and Space Astronomy

University of Colorado at Boulder, Campus Box 389

Boulder, CO 80309-0389

Adam.Jensen@colorado.edu, tsnow@casa.colorado.edu

ABSTRACT

In this paper we report on the gas-phase abundance of singly-ionized magnesium (Mg II) in 44 lines of sight, using data from the *Hubble Space Telescope* (*HST*). We measure Mg II column densities by analyzing medium- and high-resolution archival STIS spectra of the 1240 Å doublet of Mg II. We find that Mg II depletion is correlated with many line of sight parameters (e.g. $f(\text{H}_2)$, E_{B-V} , E_{B-V}/r , A_V , and A_V/r) in addition to the well-known correlation with $\langle n_{\text{H}} \rangle$. These parameters should be more directly related to dust content and thus have more physical significance with regard to the depletion of elements such as magnesium. We examine the significance of these additional correlations as compared to the known correlation between Mg II depletion and $\langle n_{\text{H}} \rangle$. While none of the correlations are better predictors of Mg II depletion than $\langle n_{\text{H}} \rangle$, some are statistically significant even assuming fixed $\langle n_{\text{H}} \rangle$. We discuss the ranges over which these correlations are valid, their strength at fixed $\langle n_{\text{H}} \rangle$, and physical interpretations.

Subject headings: ISM: abundances — ultraviolet: ISM

1. INTRODUCTION AND BACKGROUND

Magnesium is both a relatively abundant element in the Galaxy and an important component in most interstellar dust models. Mg I has an ionization potential of only 7.65 eV, while Mg II has an ionization potential of 15.04 eV. In H I regions, the dominant form of gas-phase interstellar magnesium should be Mg II. In H II regions, magnesium should

be found primarily in the form of Mg III. Gas-phase Mg I is rare, even in H₂ regions. As is the case for other elements such as silicon and iron, the average gas-phase abundance of magnesium is much smaller than the assumed overall cosmic abundance of magnesium, implying that the majority of interstellar magnesium is tied up in dust. Therefore, variations in the gas-phase magnesium abundance are only capable of having minor effects on grain composition. Nevertheless, observed variations in the gas-phase magnesium abundance may still shed light on the physical conditions of interstellar clouds.

Two major *Copernicus* surveys that included measurements of Mg II abundances and depletions were Murray et al. (1984) and Jenkins et al. (1986). Both of these studies confirmed that magnesium depletion increases with increased average hydrogen volume density, $\langle n_{\text{H}} \rangle = N(\text{H}_{\text{tot}})/r$ (where r is the line-of-sight pathlength), in the line of sight. Jenkins et al. (1986) also found several correlations between the depletions of magnesium and other elements, which they cited as secondary to the correlation between those depletions and $\langle n_{\text{H}} \rangle$. In both studies, the depletion of magnesium was not strongly correlated to other line of sight parameters, such as E_{B-V} and the magnitude of the 2175 Å extinction “bump”. We also note that there is a systematic difference in the absolute values of the abundances and depletions between these studies and more recent studies that is fairly substantial. This is due to a difference in the assumed f -values of the 1240 Å doublet of magnesium. We comment on our chosen f -values in §2.1.

More recently, Cartledge et al. (2006) also examined the abundances and depletions of Mg II and several other elements in the interstellar medium using STIS data. (Hereafter, this paper will be referred to as CLMS, for the initials of the authors.) Similar to the *Copernicus* studies, CLMS concluded that the line of sight parameter with the clearest connection to elemental depletions is the average hydrogen volume density, $\langle n_{\text{H}} \rangle$. CLMS also explored potential correlations between depletions and other line of sight parameters such as the molecular fraction of hydrogen, $f(\text{H}_2)$; selective extinction, E_{B-V} ; and selective extinction divided by line-of-sight pathlength, E_{B-V}/r . CLMS concluded that $\langle n_{\text{H}} \rangle$ was the parameter that best identified warm vs. cold clouds, and that no other parameters produced correlations with magnesium depletion that were both as strong and with as little scatter.

We began this study before CLMS was published. In spite of the similarities between that study and this one, we have proceeded with this study to provide an independent analysis of Mg II, and also because we have analyzed potential trends with respect to parameters not analyzed in CLMS, e.g. A_V and R_V . The Mg II column densities of 11 out of the 44 lines of sight in our sample have also been analyzed previously by CLMS. We still report our results in this paper for two main reasons: (1) these lines of sight provide a basis of comparison for the methods of this paper and those of CLMS and (2) these lines of sight

can be analyzed with respect to the aforementioned line of sight parameters not analyzed in CLMS. A comparison of the column density measurements for these common lines of sight is found in §2.3.

In §2 we discuss our observations and data reduction, including comments on the 1240 Å doublet and our derivation of column densities and abundances. In §3 we discuss our results, including observed correlations and a review of the Galactic abundance of magnesium. In §4 we summarize our findings.

2. OBSERVATIONS AND DATA REDUCTION

2.1. The Mg II Doublet at $\lambda\lambda 1239, 1240$

Morton (2003), summarizing several sources, cites only four major, ground-state doublets of Mg II—a strong doublet with transitions at 2795.5 Å and 2802.7 Å, a much weaker doublet at 1239.9 Å and 1240.4 Å, a doublet at 1026.0 Å and 1026.1 Å similar in strength to the 1240 Å doublet, and an even weaker doublet at 946.7 Å and 946.8 Å. STIS data sets that cover the wavelength of strong doublet near 2800 Å exist for only one of our lines of sight (HD 93205); if more data did exist, the lines would be saturated in most cases, though each line might show damping wings for a more certain derivation of column density in a few cases. The doublets at 946 Å and 1026 Å, in addition to being self-blended in *FUSE* data, are both wiped out by strong hydrogen absorption in the high-column density lines of sight in this sample (H₂ wipes out the 946 Å doublet and H I Lyman- β absorption wipes out the 1026 Å doublet).

Thus, the two lines of the 1240 Å doublet are the only absorption lines of use. Morton (2003) notes that there are converging theoretical values for the combined magnitude of the f -values of this doublet, though there is some variation between different authors in the calculated ratio of the f -values. The studies under discussion in Morton (2003) include Fleming et al. (1998), Godefroid & Froese Fischer (1999), Theodosiou & Federman (1999), and Majumder et al. (2002). Morton (2003) ultimately opts for the values by Theodosiou & Federman (1999). These sources calculate a combined f -value of the doublet that is consistent to within 0.13 dex. In keeping with Morton (2003), we elect to use the Theodosiou & Federman (1999) f -values of $f_{1239.9} = 6.32 \times 10^{-4}$ and $f_{1240.4} = 3.56 \times 10^{-4}$. CLMS also opted to use these f -values; thus, f -values are not a source of systematic error between this study and CLMS. Morton (2003) notes that despite consistency in the combined f -value of the doublet, there is some discrepancy in the f -value ratio between the two lines. However, the Theodosiou & Federman (1999) f -values represent a ratio (1.78)

that is consistent with empirical values by Fitzpatrick (1997) and Sofia et al. (2000) and the theoretical calculations of Majumder et al. (2002); these sources quote ratios between 1.74 and 1.82. Note, however, that Godefroid & Froese Fischer (1999) found a ratio of 2.54, while Fleming et al. (1998) only calculated the combined f -value of the doublet and not of the individual lines.

The damping constants of these lines are not reported in Morton (2003), but in all cases the lines are much too weak for damping constants to have a significant effect. We use this doublet exclusively for the determination of column densities. We describe our fitting methods below (§2.3), but first describe the STIS data and relevant procedures used to observe the lines.

2.2. *HST* Data

Archival STIS data are available for all 44 of the lines of sight in this study. Lines of sight were initially chosen from several literature sources in attempts to examine abundances of silicon and iron. Basic line of sight parameters (e.g. spectral types and Galactic coordinates of the background stars) are given in Table 1. A summary of the STIS data sets used is given in Table 2. Hydrogen column densities and related parameters (e.g. $f(\text{H}_2)$) are given in Table 3, while extinction and reddening parameters E_{B-V} , A_V , and R_V are given in Table 4.

We used “on-the-fly” calibrated (Micol et al. 1999) data. For observations with the E140H grating, the 1240 Å line is found in two echelle orders. We coadded these echelle orders and multiple observations where available. We performed the same fitting routines described below (§2.3) in test cases on the individual echelle orders and observations and found consistency between those results and our results for the coadded spectra.

We assumed empirically measured point-spread functions (S. V. Penton, private communication) in analyzing data that utilize the E140H and E140M gratings and various apertures. We have noted the use of this PSF in our previous work (Jensen et al. 2007; Jensen & Snow 2007). This empirical PSF is not Gaussian.

2.3. Column Density Measurements and Errors

Measurements of Mg II column densities are derived solely through measurements of the 1240 Å doublet. Assuming the f -values given in §2.1 and the PSF described in §2.2, we fit Voigt profiles simultaneously to the two lines of the doublet. The Voigt profile is

the most general absorption profile; it is inherently Gaussian for unsaturated weak lines, and inherently damped for very strong lines. The observed profile is the convolution of the inherent profile and the PSF. When the lines of the doublet are asymmetric or multiple velocity components are clearly resolved, we fit each individual component with a Voigt profile.

We fit these multiple components without any *a priori* assumptions on the overall velocity structure of the line of sight. This involves “ χ -by-eye” to first order, then comparing the reduced χ^2 of fits with a different number of components. Though high-resolution optical data on the velocity structure exist for some of these lines of sight (e.g. Pan et al. 2004; Welty & Hobbs 2001; Welty et al. 2003), the ionization potential of the species studied (K I and Ca I) is smaller than the ionization potential of Mg I (7.6 eV) and much smaller than the ionization potential of Mg II (15.1 eV), indicating that those elements and Mg II are unlikely to have high spatial coincidence. Therefore, fitting observed resolved components and asymmetries is no less—and mostly likely better—justified than assuming the velocity structure of one of these other elements.

Our profile-fitting¹code simultaneously fits the profiles of both doublet lines with a single total line-of-sight column density, and three parameters for each observed velocity component: b -value, velocity offset, and fraction of total column density. The code outputs errors for each of these parameters, though the errors on total column density are often somewhat small. To properly account for continuum placement, which should be the dominant source of error, we calculate the equivalent widths (W_λ) and errors in W_λ due to a $1\text{-}\sigma$ shift in the continuum (determined by the S/N). We then assume that the fractional error in column density is the same as the average fractional error in the W_λ of the two lines of the doublet. This is a slightly more conservative estimate of the column density error than our code otherwise produces. Two samples of the fit profiles are shown in Figure 1. Our column density results, along with derived abundances (see §2.4) and equivalent widths, are shown in Table 5.

Potential systematic errors in our methods could come from the aforementioned uncertainties in the f -values, incorrect normalization of the continuum, and concerns of unresolved or misidentified saturation. Our choice of f -values was discussed above (§2.1). As noted there, while there is some range in the theoretical values summarized by Morton (2003), two recent empirical studies determine ratios consistent with our chosen ratio of 1.78, and only one of the three theoretical values that Morton cites is inconsistent with this value. Because

¹Note that our use of the phrase “profile fitting” is different than that of CLMS, in that, as described above, we do not place any *a priori* constraints on the components that we identify.

we cannot guarantee that both components are unsaturated in most cases, we cannot independently analyze the ratio of f -values. However, we feel confident that the aforementioned data are converging toward an f -value ratio of ≈ 1.78 .

Normalizing the continuum is fairly trivial in this spectral region, as this doublet is far from any other major spectral features in most lines of sight. In a few lines of sight, broad stellar features do appear, but fitting the background spectra is still easily accomplished with the use of multiple order polynomials.

Saturation can pose a problem in two different ways. First, if there are unresolved saturated components, our fits might determine a column density that is too small. Second, if we observe a resolved saturated component, and the inherent width of the line is not much broader than the width of the PSF, the fit will be very uncertain, which could result in significant deviations from the true column density. Both of these concerns should be somewhat alleviated by the fact that our method of simultaneously fitting the profiles of both lines of the doublet constrains saturation as much as is possible given the data. This is especially true of the latter concern of misidentifying the b -value of a resolved, saturated component.

We also note that in the 11 lines of sight where we have overlapping data with CLMS, our methods produce column densities that are generally consistent with their profile fitting and apparent optical depth methods (hereafter PF and AOD, respectively). A comparison of the common lines of sight is shown in Table 6. Of the 22 comparison pairs (our results versus each method for all 11 lines of sight), 19 possess $1\text{-}\sigma$ agreement. Another two pairs (our measurements versus the AOD measurements for HD 37021 and HD37903) miss $1\text{-}\sigma$ agreement but are consistent within $2\text{-}\sigma$ and agree within $1\text{-}\sigma$ on the PF measurements. Conversely, our measurement of HD 147888 agrees with the AOD measurement of CLMS, but not with the PF measurement. CLMS note this line of sight as by far the most discrepant between the two methods in their study (0.19 dex). However, CLMS also discuss strategies for correction to the AOD method by Savage & Sembach (1991) and Jenkins (1996), the former of which brings the two methods to within 0.08 dex. CLMS elect to adopt their PF results in all cases.

These comparisons allow us to conclude that our methods are consistent with the (uncorrected) AOD method, which itself is typically consistent with the PF method of CLMS. The discrepancy for HD 147888 is well outside the norm in this regard. We also note that our equivalent widths (reported in Table 5) are consistent with equivalent widths of CLMS to within errors (though note that CLMS only report the equivalent width of the 1239.9 Å line).

2.4. Hydrogen Column Densities

In order to analyze abundances and depletions, we need to have hydrogen column densities. We define $N(\text{H}_{\text{tot}}) = [N(\text{H I}) + 2N(\text{H}_2)]$, neglecting contributions from H II regions. Given the ionization potentials of H I and Mg II (13.6 eV and 15.1 eV), it is reasonable to assume that the vast majority of magnesium is found in the form of Mg I and Mg II in H I and H₂ regions, with only a minimal amount of Mg II from H II regions contributing to the Mg II column density that we see.

The atomic hydrogen column densities are determined through profile fitting of the Lyman- α line of atomic hydrogen. The fits come from several sources, summarized in Table 3. Three stars are cooler than type B2.5: HD 27778, HD 91597, and HD 147888. Therefore, the Lyman- α fits of these lines might be subject to stellar contamination. However, in all cases, estimations of stellar Lyman- α and/or consistency checks with other methods of H I determination have been employed. For a full discussion of these, see the references in which the measurements originally appear (Cartledge et al. 2004 for HD 27778 and HD 147888; Diplas & Savage 1994 for HD 91597) or consult our previous discussions of these lines of sight (Jensen et al. 2007; Jensen & Snow 2007).

Molecular hydrogen column densities are taken from recent *FUSE* surveys and other *FUSE* data (primarily J. M. Shull et al., in preparation, but see Table 3 for all references). In these papers $N(\text{H}_2)$ is determined for each line of sight by fitting several low- J lines. Reliable FUV data do not exist for HD 37021 and HD 37061; therefore, in these two lines of sight we cannot report H₂ column densities or $f(\text{H}_2)$, and our $N(\text{H}_{\text{tot}})$ and $\langle n_{\text{H}} \rangle$ are only measures of atomic hydrogen column density and volume density, respectively. This is unfortunate, because as discussed in §3, these two lines of sight have two of the five largest depletions of any of the lines of sight in this sample. If $N(\text{H}_2)$ is large in either of these lines of sight, then they likely have the greatest depletions of all the lines of sight in this sample, perhaps by a significant amount. However, Cartledge et al. (2001) have argued that $f(\text{H}_2)$ is likely small in both of these lines of sight. This is based on observations of little or no Cl I in these lines of sight; the Cl I ionization potential of 12.97 eV implies that $N(\text{H}_2)$ is similarly small, in turn implying a small value of $f(\text{H}_2)$.

3. RESULTS AND DISCUSSION

3.1. Correlations

Our results for the column densities of Mg II are given in Table 5. The major correlation found by both Jenkins et al. (1986) and CLMS is that the depletion of magnesium and many other elements increases with overall line of sight density, $\langle n_{\text{H}} \rangle$. Both interpreted their models in light of the model by Spitzer (1985). The Spitzer model contends that the ISM contains two distinct varieties of cloud (warm and cold), each with a distinct depletion level. In this model, lines of sight with average densities of a few-tenths of a particle per cm^{-3} are largely sampling the warm ISM, while lines of sight with average densities of a few particles per cm^{-3} are largely sampling the cold ISM. This explains the observed plateaus of depletion at both low and high densities, with a transition near average densities of $\sim 1 \text{ cm}^{-3}$, where lines of sight are sampling both types of clouds. This model, however, does not take into account the transition to a much different regime of cloud chemistry expected for translucent clouds (for a recent review, see Snow & McCall 2006).

Jenkins et al. (1986) also found evidence of lesser correlations between the depletion of various elements and other parameters of reddening and extinction, but concluded that these correlations were secondary to the correlation with $\langle n_{\text{H}} \rangle$. CLMS examined the depletion of Mg II compared to $f(\text{H}_2)$, E_{B-V} , and E_{B-V}/r . CLMS concluded that only E_{B-V}/r provided a correlation with magnesium depletion that was as at least roughly as significant as the correlation with $\langle n_{\text{H}} \rangle$, but with increased scatter.

However, in our recent work (Jensen & Snow 2007), we explored the possibility of correlations between iron depletion and various other line of sight parameters. We found very similar correlations between iron depletion and measures of dust density (E_{B-V}/r and A_V/r) and the molecular fraction of hydrogen ($f(\text{H}_2)$). We also examined iron depletion as a function of R_V , the ratio of total visual extinction to selective extinction, though a conclusive trend did not present itself. Using many of the same lines of sight in this paper as in Jensen & Snow (2007), we find the same correlations generally hold with respect to magnesium depletion. In what follows, we discuss the nature of these correlations and possible interpretations.

3.1.1. Correlations with Hydrogen

First, we note that magnesium depletion is clearly correlated with total hydrogen volume density $\langle n_{\text{H}} \rangle$. Five lines of sight (HD 27778, HD 37021, HD 37061, HD 37903, and HD

147888) have substantially larger depletions than any of the other lines of sight in this sample; HD 27778, HD 37021, HD 37061, and HD 147888 are the four densest lines of sight (in terms of $\langle n_{\text{H}} \rangle$), while the density of HD 37903 is in the top 20% of our sample. This correlation is plotted in Figure 2. Since these dense lines of sight are also some of the lines of sight that are found in both our sample and that of CLMS, we are not probing significantly higher average density and cannot expand on their conclusions regarding $\langle n_{\text{H}} \rangle$.

We also find that magnesium depletion is correlated with total hydrogen column density. However, we conclude that this is primarily a secondary correlation due to the correlation with $\langle n_{\text{H}} \rangle$. However, we can attempt to analyze whether or not the correlation is independently significant. To do this, we follow the methods described in Jenkins et al. (1986). First, we calculate Pearson correlation coefficients between depletion and the two variables of interest (in this case $\log N(\text{H}_{\text{tot}})$ and $\log \langle n_{\text{H}} \rangle$), as well as those two variables with each other. The partial correlation coefficient is then given by $\rho_{12.3} = (\rho_{12} - \rho_{13}\rho_{23}) / [(1 - \rho_{13}^2)(1 - \rho_{23}^2)]^{-1/2}$, where the subscripts on the correlation coefficients indicate the two variables being correlated, and $\rho_{12.3}$ is the correlation coefficient between the first two variables if the third variable is held fixed. However, what is really being calculated is r , the sample correlation coefficient(s), as opposed to ρ , the population correlation coefficient(s). Once $r_{12.3}$ has been calculated, we examine the significance level for a t -test of the appropriate number of degrees of freedom (in this case, the number of data points minus three) to determine the probability that ρ is non-zero (i.e. a true correlation exists). Using these methods, we find a 49% chance of the null hypothesis (i.e. the two-sided probability that $\rho = 0$) for a correlation between Mg II depletion and $N(\text{H}_{\text{tot}})$ when $\langle n_{\text{H}} \rangle$ is held fixed.

Because this technique of trivariate analysis uses Pearson correlation coefficients, a few caveats apply, namely that linear relationships and normal distributions are implicitly assumed. We used $\log(\text{Mg II}/\text{H})$, $\log N(\text{H}_{\text{tot}})$, and $\log \langle n_{\text{H}} \rangle$ in the analysis just discussed because the correlation between all combinations of those variables are stronger than when in linear form.

CLMS also explored possible correlations between magnesium depletion and $f(\text{H}_2)$, but only briefly commented on the results. They concluded that any correlation was less significant than the correlation between magnesium depletion and $\langle n_{\text{H}} \rangle$, in that it did not as effectively discriminate between the distinct depletion levels expected in the Spitzer (1985) model. The upper right panel of Figure 9 in CLMS shows a very clear correlation between magnesium depletion and $f(\text{H}_2)$ for $f(\text{H}_2) \gtrsim 0.1$, superimposed with a scatter plot in depletion for a smaller subset of lines with $0.01 \lesssim f(\text{H}_2) \lesssim 0.1$. Two additional lines of sight with $f(\text{H}_2) \lesssim 10^{-4}$ conform to the main correlation in that they show minimal depletion.

We also see a clear correlation between magnesium depletion and the molecular fraction of hydrogen, $f(\text{H}_2)$, plotted in Figure 3, with depletion increasing with increasing $f(\text{H}_2)$. There is the exception of one discrepant point, HD 147888, that exhibits substantial depletion at $f(\text{H}_2) \sim 0.1$. We note that CLMS found a larger column density for this line of sight than we do (0.2 dex); however, even if we adopt the CLMS Mg II column density for this line of sight, its abundance is still 0.26 dex smaller than any line of sight in our sample with $f(\text{H}_2) < 0.4$.

We concur with CLMS that the correlation between magnesium depletion and $f(\text{H}_2)$ is not as rigorous as the correlation with $\langle n_{\text{H}} \rangle$. We examine the data using various combinations of the variables in their logarithmic (where correlations are the strongest) and linear forms. In all cases, we find that the probability of the null hypothesis (i.e. $\rho = 0$, as discussed above) between Mg II depletion and $f(\text{H}_2)$ with $\langle n_{\text{H}} \rangle$ held constant is less than 5%; in most cases, it is $\lesssim 1\%$. Conversely, the probability that there is no correlation between Mg II depletion and $\langle n_{\text{H}} \rangle$ with $f(\text{H}_2)$ held constant is less than 0.1%. Therefore, we conclude that while $\langle n_{\text{H}} \rangle$ is clearly the dominant correlation, the correlation with $f(\text{H}_2)$ has some independent significance.

A question of interest is where scatter seems to be introduced and why. Between Figure 9 of CLMS and Figure 3 of this paper, scatter is only observed at $f(\text{H}_2) \lesssim 0.1$. In our recent related work on Fe II (Jensen & Snow 2007), we note that Fe II depletion is also correlated with $f(\text{H}_2)$, but there are a few exceptions to the trend at both high and low values of $f(\text{H}_2)$. The most severe exceptions noted in that paper were HD 147888 and HD 164740 (with large depletions but $f(\text{H}_2) \lesssim 0.1$) and HD 210121 (with less depletion despite $f(\text{H}_2) \sim 0.7$). For Mg II, however, we do not see any outlying points at values of $f(\text{H}_2)$ larger than ~ 0.1 within either this sample or CLMS. Points such as HD 147888, however, still require explanation.

Snow (1983) put forth the possibility that in some dense environments an increased average grain size, which decreases the grain surface area per unit volume, may suppress H_2 formation (as H_2 is thought to form on grain surfaces). This scenario was specifically discussed in the context of the ρ Oph cloud, for which there is independent evidence (in part, a value of R_V greater than the interstellar average of 3.1) that grain coagulation has occurred. Our main outlying line of sight, HD 147888 (with R_V of 4.06), passes through the ρ Oph cloud, so observing the combination of a dense, depleted environment with small $f(\text{H}_2)$ is not surprising in this case.

Two of the other lines of sight with large depletions are HD 37021 and HD 37061. Reliable far-ultraviolet data sets do not exist for these lines of sight; therefore, they do not have measurements of the molecular hydrogen column densities or subsequently derived molecular fractions of hydrogen. However, as stated above in §2.4, Cartledge et al. (2001)

has argued that these lines of sight have small values of $f(\text{H}_2)$ based on a lack of Cl I. These two lines of sight also have large values of R_V (5.54 and 4.23, respectively), implying a larger average grain size. The possible effect of grain size on depletions and H_2 formation, and other interpretations, will be discussed further in §3.1.2.

Barring such outlying points, the trend of increased Mg II depletion with increased $f(\text{H}_2)$ has a relatively clear interpretation. H_2 is formed in the same dense, dusty environments that foster large depletions. Within the context of this sample and CLMS, this seems to hold for lines of sight with $f(\text{H}_2) \gtrsim 0.1$. While the ubiquity of H_2 even in diffuse regions complicates the issue (see conclusions of Rachford et al. 2002), there is still a physical argument that $f(\text{H}_2)$ should be a good diagnostic of the local conditions of interstellar clouds, and therefore depletions. It is worth noting that the similar trend between iron depletion and $f(\text{H}_2)$ exhibits scatter up to $f(\text{H}_2) \sim 0.3$ in the work of Savage & Bohlin (1979), in addition to the outlying points mentioned above from Jensen & Snow (2007). Whether the range in $f(\text{H}_2)$ over which there is scatter in the abundances is truly different for magnesium and iron or is simply a selection effect is unclear.

3.1.2. Correlations with Extinction and Reddening Parameters

We find that the depletion of Mg II is correlated to both selective extinction, E_{B-V} , and total visual extinction, A_V . However, there is significant scatter in these correlations. Because these are integrated line of sight parameters, it makes sense to divide by line-of-sight pathlength. Both E_{B-V} and A_V are strongly correlated with $N(\text{H}_{\text{tot}})$, and both are thought to be rough measures of the total dust column density. Therefore, E_{B-V}/r and A_V/r should be strongly correlated with $\langle n_{\text{H}} \rangle$ and be approximations of the total dust volume density. When we look for correlations between magnesium depletion and E_{B-V}/r and A_V/r we find that the correlations are substantially increased when compared to the integrated line of sight parameters. Therefore, we can say, with reasonable confidence, that magnesium depletion is increased in increasingly dusty environments. The correlations with E_{B-V}/r and A_V/r are plotted in Figures 4 and 5.

As with the correlation between depletion and $f(\text{H}_2)$, we examine partial correlation coefficients to determine the independent significance of these correlations. The partial correlation coefficient between Mg II depletion and $\log E_{B-V}/r$ with $\log \langle n_{\text{H}} \rangle$ held fixed implies that the probability of the null hypothesis is less than 6%. The same partial correlation coefficient with $\log A_V/r$ implies that there is less than a 1% chance of the null hypothesis. (Note that both probabilities are two-sided to a t -distribution.) We consider these variables in their logarithmic forms because these are the versions of the variables that exhibit the

strong correlations (for all combinations of the variables in question). However, if the variables are considered in non-logarithmic forms, the probability of the null hypothesis generally increases. Again we note that this type of trivariate statistical measure implicitly assumes that the correlation is linear with normally distributed scatter. As with the correlation between depletion and $f(\text{H}_2)$, we conclude that while these correlations do not improve on $\langle n_{\text{H}} \rangle$ as a predictor of depletions, this is limited evidence that they are significant in their own right.

We have briefly explored the possibility that the additional (or “missing”) magnesium that is depleted from these lines of sight is found in the form of gas-phase Mg I in regions that are presumably shielded from radiation by dust. While the STIS data do not cover Mg I absorption lines in many cases, our results indicate that gas-phase Mg I column densities are far too small to account for the order-of-magnitude increase in depletion seen in gas-phase Mg II. Therefore, it is likely that the missing gas-phase magnesium is tied up in the additional grains found in these environments, supporting the conclusion above that the correlations between Mg II depletion and the parameters $\log E_{B-V}/r$ and $\log A_V/r$ are physically significant. It is also worth noting that in no case do we see Mg/H less than ~ 1 ppm, even in the densest environments, with values of E_{B-V}/r and A_V/r several times larger than the average of the sample. This suggests that these lines of sight are not probing what might be considered “translucent clouds” (though some may be “translucent lines of sight”; see Snow & McCall 2006).

The Mg II abundance is plotted against the ratio of total visual to selective extinction, $R_V \equiv A_V/E_{B-V}$, in Figure 6. The plot shows significant scatter; however, some statistical measures show the possibility of a slight correlation. A Pearson correlation coefficient between $\log(\text{Mg II}/\text{H})$ and R_V implies that the probability of the null hypothesis is about 31%. A Spearman’s ρ rank correlation coefficient, which does not depend on the functional form assumed (including whether variables are considered linearly or logarithmically) beyond assuming that the correlation is either monotonically increasing or monotonically decreasing, shows a negative correlation (decreasing abundance/increasing depletion as R_V increases) and is significant to approximately $1.3\text{-}\sigma$. Therefore, there is evidence of a possible slight correlation between depletion and R_V . However, this is far from a certain conclusion. Significant selection effects are also a possibility, as the correlations are dominated by some of the points that have greater depletion and large values of R_V . In fact, if these lines of sight are excluded, the trend begins to reverse toward a positive correlation between increasing Mg II abundance and increasing R_V . In general, we conclude that R_V is a poor predictor of depletions; as one anecdotal counterexample, HD 91597 has a very large value of $R_V = 4.9$ but does not exhibit particularly large Mg II depletion.

However, there are a few lines of sight that present interesting interpretive challenges where the value of R_V may provide insight. As discussed above, the possibility of large magnesium depletion but small $f(\text{H}_2)$ exists for three lines of sight: HD 37021, HD 37061, and HD 147888. In the latter case the effect is clear, while in the former two cases the small value of $f(\text{H}_2)$ is merely inferred. What is interesting, as noted above, is that these three lines of sight all have values of $R_V > 4$ which is a fairly significant deviation from the interstellar average of 3.1. Because large grains contribute to A_V (i.e. grey extinction) but less so to E_{B-V} , R_V is thought to be correlated to average grain size. Explaining why depletion should increase in a line of sight with large grains is difficult. As mentioned above in our discussion of H_2 and iron depletion, increased grain size decreases dust surface area per unit volume, and therefore reduces H_2 formation rates. However, decreased surface area per unit volume also implies a reduction in rates of sticking between dust grains and gas-phase atoms.

It seems we can reasonably conclude that the large values of R_V , i.e. the larger average grain populations, are not responsible for the large depletions by way of atoms and ions sticking to the grains. One possibility is that the large depletions are instead “locked in” prior to grain coagulation. Another possibility is the effect of a high-radiation field: this is known for the line of sight toward HD 147888 (ρ Oph D) as well as HD 37021 and HD 37061 which are in Orion (radiation is presumed to be responsible for the relative lack of Cl I, and thus also H_2 , as mentioned in §2.4). However, Snow (1983) argues that the increased radiation is unlikely to be entirely responsible for the low $f(\text{H}_2)$ in the ρ Oph cloud. Whether or not this is the case for HD 37021 and HD 37061 is unclear. More details about the radiation field and the exact nature of the grain population (we have only considered the crude measure of R_V) are probably necessary to fully understand these lines of sight.

3.1.3. *Anticorrelation with Distance*

We find that magnesium depletion is generally anticorrelated with distance to the background star, that is, line of sight pathlength; this relationship is shown in Figure 7. Depletion decreases by nearly an order of magnitude between very short lines of sight and those up to about 2 kpc or so, and then is relatively constant (to within about 0.3-0.4 dex) out to about 6 kpc. As we concluded for a similar anticorrelation seen between iron depletion and distance (Jensen & Snow 2007), the long pathlengths are likely sampling a variety of cloud conditions, resulting in the constant depletion for long-pathlength lines of sight. On the other hand, given the comparable hydrogen column densities of all the lines of sight in this study ($\log N(\text{H}_{\text{tot}}) \approx 21 - 22$), the shorter lines of sight are generally the denser lines of sight.

3.1.4. *Spatial Variations*

We find one very interesting correlation with Galactic location: the five stars with the largest depletions reside at higher Galactic latitudes of $|b| > 15^\circ$. However, with pathlengths of less than 1 kpc, these lines of sight are still primarily in the Galactic disk. When we analyze magnesium depletions against the height from the center of the Galactic disk, $z = r \sin b$, we do not see a strong correlation. The variation with respect to Galactic latitude is most likely a coincidence, given that these are some of the densest and most reddened lines of sight. We do not see any other evidence of significant spatial variations.

3.2. Mg/H of Galactic Stars

In the last several years, three major papers have attempted to analyze the cosmic abundance “standards” in the ISM through studies of stellar abundances and meteoritic abundances—Snow & Witt (1996), Sofia & Meyer (2001), and Lodders (2003). The importance of these standards is to compare them with the observed gas-phase abundances and infer an absolute value for depletions—and therefore absolute values for the amount of these elements in phases other than atomic gas, i.e. dust grains and molecules.

Of the major elements relevant to dust, the element with the best determined cosmic abundance is iron. The four major measurements of the cosmic Fe/H ratio—solar, B stars, F and G stars, and CI chondrites—all agree very closely, largely within the errors. The situation is somewhat more complex for other elements. Carbon and oxygen show apparent overabundances in the Sun compared to F and G stars (whether or not the solar and F/G star abundances potentially agree within the errors depends on the choice of solar abundances, regarding which there is still some uncertainty), while B stars show relative deficits in these abundances compared to the Sun and other F and G stars. The chondritic abundances of C and O are even smaller. Nitrogen seems to be somewhat less abundant in B stars than in the Sun, though the two are reconcilable within the errors; F and G nitrogen abundances are generally unknown, and the chondritic abundances are substantially lower. Silicon seems to be most abundant in F and G stars, slightly less abundant in the Sun, and about half as abundant in B stars. The errors, however, do not rule out agreement between all three measurements. However, the chondritic abundance tightly matches the solar abundance.

Both Sofia & Meyer (2001) and Lodders (2003), cite Holweger (2001) for the solar abundance of magnesium, $\log(\text{Mg}/\text{H}) = -4.46$; Snow & Witt (1996) report a slightly older value from Anders & Grevesse (1989) of $\log(\text{Mg}/\text{H}) = -4.42$, though these values are consistent within the errors. The chondritic abundances in Lodders (2003) of $\log(\text{Mg}/\text{H}) = -4.44$ are

also very consistent with these solar values. The discrepancy arises when various stellar abundances are considered. Both Snow & Witt (1996) and Sofia & Meyer (2001) found significantly smaller abundances of Mg for B stars. Snow & Witt (1996) found $\log(\text{Mg}/\text{H}) = -4.63$ for field B stars and $\log(\text{Mg}/\text{H}) = -4.68$ for cluster B stars; Sofia & Meyer (2001), making no distinction between cluster and field stars, found $\log(\text{Mg}/\text{H}) = -4.64$ for all B stars. Though there is marginal agreement within the very large errors in these numbers, the B star abundances are $\approx 60\%$ smaller than the solar abundances. Snow & Witt (1996) and Sofia & Meyer (2001) also disagree on the Mg abundance in F and G stars ($\log(\text{Mg}/\text{H}) = -4.52$ and -4.37 , respectively) due most likely to Sofia & Meyer (2001) restricting their sample to stars with ages of ≤ 2 Gyr. Again, however, these values have relatively large errors and are reconcilable with the B star abundances, though just barely.

What effect does the choice of a cosmic magnesium abundance have for the implied dust-phase abundances to be used in dust models? The differences between the cosmic abundances just discussed leads to nontrivial differences in the dust-phase abundances. Our weighted interstellar average of Mg II/H is 2.7 ± 0.1 ppm (parts per million), though the median value in our 44 lines of sight is somewhat larger at 6.2 ppm. Taking the extremes of the above numbers, anywhere between ~ 20 and ~ 40 ppm of Mg is available for creating dust. Examining the various models compared in Table 3 of Snow & Witt (1996), we find that most models require much more Mg than the lower value of ~ 20 implied by a B star abundance standard. That a B star abundance is less likely to represent the cosmic abundance was also found by Zubko et al. (2004), who had more difficulty fitting dust models to observations using the dust-phase abundances implied by assuming B star abundances as the cosmic standard. In fact, this is true even though Zubko et al. assumed ≈ 0 ppm of magnesium to be in the gas-phase. If the few ppm of magnesium in the gas-phase as measured by this paper and CLMS were included, the Zubko et al. (2004) fits would become even more strained (the best fits for B star abundances were at the limit of the error in those abundances and inferior to the fits obtained using other abundances). Therefore, the major conclusion that we can make regarding cosmic abundances and the incorporation of magnesium into dust is to add to the evidence that B star abundances, despite B stars being younger and therefore potentially good tracers of the current ISM, are a poor cosmic standard. Whether or not the solar or an F and G star abundance standard for Mg is a better fit is a test that is too sensitive for us to comment on, given the uncertainties in those abundances.

4. SUMMARY

We have analyzed the abundance of Mg II in 44 lines of sight. Our study does not probe substantially larger average hydrogen volume densities than previously observed by CLMS; therefore, we observe the same correlations between Mg II and the $\langle n_{\text{H}} \rangle$ and E_{B-V}/r . We also note a correlations between magnesium depletion and A_V/r , a different measure of dust density. Correlations between $N(\text{H}_{\text{tot}})$ and the reddening and extinction parameters E_{B-V} and A_V mean that correlations between Mg II depletion and dust density measures are expected. However, these latter correlations, while not strong than the correlation between depletion and $\langle n_{\text{H}} \rangle$, show some evidence of being significant even at fixed $\langle n_{\text{H}} \rangle$ and should be more directly related to the line-of-sight dust content. We also note a correlation between magnesium depletion and $f(\text{H}_2)$ in our data; combined with the results of CLMS, this correlation seems to be valid for $f(\text{H}_2) \gtrsim 0.1$ but not at smaller $f(\text{H}_2)$. A question that is related to the trend with $f(\text{H}_2)$ is why so little H_2 forms in certain high-density lines of sight. Our results are consistent with the Snow (1983) suggestion that the reduced grain surface area per unit volume of large grains plays a role in reducing H_2 formation rates. For similar reasons, we can conclude that the grain coagulation probably occurs after depletions are already “locked into” the dust, rather than depletion of gas-phase atoms onto grain surfaces.

The authors would like to thank the anonymous referee for many helpful comments that greatly improved the manuscript. The authors also wish to thank S. V. Penton for the use of his measurements of the STIS point-spread functions; B. A. Keeney for the original version of the profile-fitting code that we adapted to our purposes; and J. M. Shull and B. L. Rachford for the use of their unpublished measurements of molecular hydrogen column densities. This work was supported by NASA grant NAG5-12279.

REFERENCES

- Aiello, S., Barsella, B., Chlewicki, G., Greenberg, J. M., Patriarchi, P., & Perinotto, M. 1988, *A&AS*, 73, 195
- Anders, E., & Grevesse, N. 1989, *Geochim. Cosmochim. Acta*, 53, 197
- André, M. K., Oliveira, C. M., Howk, J. C., Ferlet, R., Désert, J.-M., Hébrard, G., Lacour, S., Lecavelier des Étangs, A., Vidal-Madjar, A., & Moos, H. W. 2003, *ApJ*, 591, 1000
- Cartledge, S. I. B., Lauroesch, J. T., Meyer, D. M., & Sofia, U. J. 2004, *ApJ*, 613, 1037
- . 2006, *ApJ*, 641, 327

- Cartledge, S. I. B., Meyer, D. M., Lauroesch, J. T., & Sofia, U. J. 2001, *ApJ*, 562, 394
- Diplas, A., & Savage, B. D. 1994, *ApJS*, 93, 211
- Fitzpatrick, E. L. 1997, *ApJ*, 482, L199
- Fleming, J., Hibbert, A., Bell, K. L., & Vaeck, N. 1998, *MNRAS*, 300, 767
- Garmany, C. D., & Stencel, R. E. 1992, *A&AS*, 94, 211
- Godefroid, M., & Froese Fischer, C. 1999, *Journal of Physics B Atomic Molecular Physics*, 32, 4467
- Holweger, H. 2001, in *AIP Conf. Proc. 598: Joint SOHO/ACE workshop "Solar and Galactic Composition"*, ed. R. F. Wimmer-Schweingruber, 23
- Hoopes, C. G., Sembach, K. R., Hébrard, G., Moos, H. W., & Knauth, D. C. 2003, *ApJ*, 586, 1094
- Jenkins, E. B. 1996, *ApJ*, 471, 292
- Jenkins, E. B., Savage, B. D., & Spitzer, Jr., L. 1986, *ApJ*, 301, 355
- Jensen, A. G., Rachford, B. L., & Snow, T. P. 2007, *ApJ*, 654, 955
- Jensen, A. G., & Snow, T. P. 2007, *ApJ*, submitted
- Lodders, K. 2003, *ApJ*, 591, 1220
- Majumder, S., Merlitz, H., Gopakumar, G., Das, B. P., Mahapatra, U. S., & Mukherjee, D. 2002, *ApJ*, 574, 513
- Micol, A., Durand, D., Pirenne, B., Gaudet, S., & Hodge, P. 1999, in *ASP Conf. Ser. 172: Astronomical Data Analysis Software and Systems VIII*, ed. D. M. Mehringer, R. L. Plante, & D. A. Roberts, 191
- Morton, D. C. 2003, *ApJS*, 149, 205
- Murray, M. J., Dufton, P. L., Hibbert, A., & York, D. G. 1984, *ApJ*, 282, 481
- Neckel, T., Klare, G., & Sarcander, M. 1980, *Bulletin d'Information du Centre de Données Stellaires*, 19, 61
- Pan, K., Federman, S. R., Cunha, K., Smith, V. V., & Welty, D. E. 2004, *ApJS*, 151, 313

- Rachford, B. L., Snow, T. P., Tumlinson, J., Shull, J. M., Blair, W. P., Ferlet, R., Friedman, S. D., Gry, C., Jenkins, E. B., Morton, D. C., Savage, B. D., Sonnentrucker, P., Vidal-Madjar, A., Welty, D. E., & York, D. G. 2002, *ApJ*, 577, 221
- Savage, B. D., & Bohlin, R. C. 1979, *ApJ*, 229, 136
- Savage, B. D., Massa, D., Meade, M., & Wesselius, P. R. 1985, *ApJS*, 59, 397
- Savage, B. D., & Sembach, K. R. 1991, *ApJ*, 379, 245
- Snow, T. P. 1983, *ApJ*, 269, L57
- Snow, T. P., Destree, J. D., & Jensen, A. G. 2007, *ApJ*, 655, 285
- Snow, T. P., & McCall, B. J. 2006, *ARA&A*, 44, 367
- Snow, T. P., & Witt, A. N. 1996, *ApJ*, 468, L65
- Sofia, U. J., Fabian, D., & Howk, J. C. 2000, *ApJ*, 531, 384
- Sofia, U. J., & Meyer, D. M. 2001, *ApJ*, 554, L221
- Spitzer, L. 1985, *ApJ*, 290, L21
- Theodosiou, C. E., & Federman, S. R. 1999, *ApJ*, 527, 470
- Welty, D. E., & Hobbs, L. M. 2001, *ApJS*, 133, 345
- Welty, D. E., Hobbs, L. M., & Morton, D. C. 2003, *ApJS*, 147, 61
- Zubko, V., Dwek, E., & Arendt, R. G. 2004, *ApJS*, 152, 211

Table 1. Lines of Sight: Stellar Data

Star Name	Spectral Class	l	b	Distance (pc)	Ref.
BD +35°4258	B0.5Vn	77.19	-4.74	3100	1
CPD -59°2603	O7V...	287.59	-0.69	2630	2
HD 12323	O9V	132.91	-5.87	3900	1
HD 13745	O9.7II((N))	134.58	-4.96	1900	1
HD 15137	O9.5V	137.46	+7.58	3300	2
HD 27778	B3V	172.76	-17.39	223	3
HD 37021	B0V	209.01	-19.38	450	4
HD 37061	B1V	208.92	-19.27	580	5
HD 37903	B1.5V	206.85	-16.54	910	5
HD 40893	B0IV	180.09	+4.34	2800	5
HD 66788	O8/O9Ib	245.43	+2.05
HD 69106	B1/B2II	254.52	-1.33	1600	5
HD 91597	B7/B8IV/V	286.86	-2.37	6400	5
HD 91651	O9VP:	286.55	-1.72	3500	1
HD 92554	O9.5III	287.60	-2.02	6795	2
HD 93205	O3V	287.57	-0.71	2600	1
HD 93222	O7III((f))	287.74	-1.02	2900	1
HD 93843	O6III(f)	228.24	-0.90	2700	1
HD 94493	B0.5Ib	289.01	-1.18	2900	5
HD 99857	B1Ib	294.78	-4.94	3058	2
HD 99890	B0.5V:	291.75	+4.43	3070	2
HD 103779	B0.5II	296.85	-1.02	3500	5
HD 104705	B0.5III	297.45	-0.34	3500	5
HD 109399	B1Ib	301.71	-9.88	1900	5
HD 116781	O9/B1(I)E	307.05	-0.07
HD 122879	B0Ia	312.26	+1.79	4800	5
HD 124314	O7	312.67	-0.42	1100	1
HD 147888	B3/B4V	353.65	+17.71	136	3
HD 152590	O7.5V	344.84	+1.83	1800	4
HD 168941	B0III/IV	5.82	-6.31	5000	5
HD 177989	B2II	17.81	-11.88	5100	5
HD 185418	B0.5V	53.60	-2.17	950	5
HD 192639	O7.5IIIF	74.90	+1.48	1100	5
HD 195965	B0V	85.71	+5.00	1300	5
HD 202347	B1V	88.22	-2.08	1300	1
HD 203374	B0IVpe	100.51	+8.62	820	2
HD 206267	O6(F)	99.29	+3.74	1000	4
HD 207198	O9II	103.14	+6.99	1000	5
HD 207308	B0.5V	103.11	+6.82
HD 207538	O9.5V	101.60	+4.67	880	5
HD 209339	BOIV	104.58	+5.87	1100	1
HD 210839	O6e	103.83	+2.61	505	3
HD 224151	B0.5IISBV	115.44	-4.64	1355	2
HD 303308	O3V	287.59	-0.61	2630	2

References. — Spectral classes and Galactic coordinates compiled from SIMBAD database at <http://simbad.u-strasbg.fr/simbad/sim-fid>. References for distances: (1) Savage et al. (1985). (2) Diplas & Savage (1994). (3) Hipparcos 4- σ —Hipparcos parallax of 4- σ precision or better. (4) Member of an OB association, cluster, or multiple-star system, DIB database at <http://dib.uiuc.edu>; values compiled from the literature or derived by L. M. Hobbs. (5) Spectroscopic distance modulus from the DIB database.

Table 2. Lines of Sight: STIS Data Sets Used

Star Name	Data Set(s)	Grating	Aperture ^a
BD +35°4258	O6LZ89010	E140M	0.2X0.2
CPD -59°2603	O4QX03010	E140H	0.2X0.09
HD 12323	O63505010	E140M	0.2X0.2
HD 13745	O6LZ05010	E140M	0.2X0.2
HD 15137	O5LH02010	E140H	0.1X0.03
	O5LH02020		
	O5LH02030		
	O5LH02040		
HD 27778	O59S01010	E140H	0.2X0.09
	O59S01020		
HD 37021	O59S02010	E140H	0.2X0.09
HD 37061	O59S03010	E140H	0.1X0.03
HD 37903	O59S04010	E140H	0.2X0.09
HD 40893	O8NA02010	E140H	0.2X0.2
	O8NA02020		
HD 66788	O6LZ26010	E140M	0.2X0.2
HD 69106	O5LH03010	E140H	0.1X0.03
	O5LH03020		
HD 91597	O6LZ32010	E140M	0.2X0.2
HD 91651	O6LZ34010	E140M	0.2X0.2
HD 92554	O6LZ36010	E140M	0.2X0.2
HD 93205	O4QX01010	E140H	0.2X0.09
HD 93222	O4QX02010	E140H	0.2X0.09
HD 93843	O5LH04010	E140H	0.1X0.03
	O5LH04020		
HD 94493	O54306010	E140H	0.1X0.03
HD 99857	O54301010	E140H	0.1X0.03
	O54301020		
	O54301030		
HD 99890	O6LZ45010	E140M	0.2X0.2
HD 103779	O54302010	E140H	0.1X0.03
HD 104705	O57R01010	E140H	0.2X0.09
HD 109399	O54303010	E140H	0.1X0.03
HD 116781	O5LH05010	E140H	0.1X0.3
	O5LH05020		
HD 122879	O5LH07010	E140H	0.1X0.03
	O5LH07020		
HD 124314	O54307010	E140H	0.1X0.03
HD 147888	O59S05010	E140H	0.2X0.09
HD 152590	O8NA04010	E140H	0.2X0.2
	O8NA04020		
	O5C08P010		
HD 168941	O6LZ81010	E140M	0.2X0.2
HD 177989	O57R03010	E140H	0.2X0.09
	O57R03020		
HD 185418	O5C01Q010	E140H	0.2X0.2

Table 2—Continued

Star Name	Data Set(s)	Grating	Aperture ^a
HD 192639	O5C08T010	E140H	0.2X0.2
HD 195965	O6BG01010	E140H	0.1X0.03
HD 202347	O5G301010	E140H	0.1X0.03
HD 203374	O5LH08010	E140H	0.1X0.03
	O5LH08020		
	O5LH08030		
HD 206267	O5LH09010	E140H	0.1X0.03
	O5LH09020		
HD 207198	O59S06010	E140H	0.2X0.09
	O59S06020		
HD 207308	O63Y02010	E140M	0.2X0.06
	O63Y02020		
HD 207538	O63Y01010	E140M	0.2X0.06
	O63Y01020		
HD 209339	O5LH0B010	E140H	0.1X0.03
	O5LH0B020		
HD 210839	O54304010	E140H	0.1X0.03
HD 224151	O54308010	E140H	0.1X0.03
HD 303308	O4QX04010	E140H	0.2X0.09

^aAperture is length X width of the slit, with both values in arcseconds.

Table 3. Lines of Sight: Hydrogen Data

Line of Sight	$\log N(\text{H I})$	Ref.	$\log N(\text{H}_2)$	Ref.	$\log N(\text{H}_{\text{tot}})$	$\langle n_{\text{H}} \rangle$	$f(\text{H}_2)$
BD +35°4258	21.28 ± 0.10	1	19.56 ± 0.03	2	21.30 ± 0.10	0.21	0.04
CPD -59°2603	21.46 ± 0.07	3	20.16 ± 0.03	2	21.50 ± 0.06	0.39	0.09
HD 12323	21.18 ± 0.09	4	20.32 ± 0.08	4	21.29 ± 0.07	0.16	0.22
HD 13745	21.25 ± 0.10	3	20.47 ± 0.05	2	21.37 ^{+0.08} _{-0.07}	0.40	0.25
HD 15137	21.11 ± 0.16	3	20.27 ± 0.03	2	21.22 ^{+0.13} _{-0.12}	0.16	0.22
HD 27778	21.10 ± 0.12	4	20.79 ± 0.06	5	21.40 ^{+0.07} _{-0.06}	3.62	0.49
HD 37021	21.68 ± 0.12	4	...	0	21.68 ± 0.12	3.45	...
HD 37061	21.73 ± 0.09	4	...	0	21.73 ± 0.09	3.00	...
HD 37903	21.17 ± 0.10	3	20.92 ± 0.06	6	21.50 ^{+0.06} _{-0.05}	1.12	0.53
HD 40893	21.50 ± 0.10	7	20.58 ± 0.05	6	21.59 ± 0.08	0.45	0.19
HD 66788	21.23 ± 0.10	1	19.72 ± 0.03	2	21.26 ± 0.09	...	0.06
HD 69106	21.08 ± 0.06	3	19.73 ± 0.05	2	21.12 ^{+0.06} _{-0.05}	0.27	0.08
HD 91597	21.40 ± 0.06	3	19.70 ± 0.05	2	21.42 ± 0.06	0.13	0.04
HD 91651	21.15 ± 0.06	3	19.07 ± 0.03	2	21.16 ± 0.06	0.13	0.02
HD 92554	21.28 ± 0.10	3	18.93 ± 0.05	2	21.28 ± 0.10	0.09	0.01
HD 93205	21.38 ± 0.05	8	19.75 ± 0.03	2	21.40 ± 0.05	0.31	0.04
HD 93222	21.40 ± 0.07	8	19.77 ± 0.03	2	21.42 ± 0.07	0.29	0.04
HD 93843	21.33 ± 0.08	3	19.61 ± 0.03	2	21.35 ± 0.08	0.27	0.04
HD 94493	21.08 ± 0.05	8	20.12 ± 0.05	9	21.17 ± 0.04	0.16	0.18
HD 99857	21.24 ± 0.08	8	20.25 ± 0.05	2	21.32 ± 0.07	0.22	0.17
HD 99890	20.93 ± 0.13	3	19.47 ± 0.05	2	20.96 ± 0.12	0.10	0.06
HD 103779	21.16 ± 0.10	3	19.82 ± 0.05	2	21.20 ± 0.09	0.15	0.08
HD 104705	21.11 ± 0.07	3	19.99 ± 0.03	2	21.17 ± 0.06	0.14	0.13
HD 109399	21.11 ± 0.06	3	20.04 ± 0.20	1	21.18 ± 0.06	0.26	0.15
HD 116781	21.18 ± 0.10	1	20.08 ± 0.05	2	21.24 ± 0.09	...	0.14
HD 122879	21.26 ± 0.12	4	20.24 ± 0.09	4	21.34 ± 0.10	0.15	0.16
HD 124314	21.34 ± 0.10	3	20.47 ± 0.03	2	21.44 ± 0.08	0.82	0.21
HD 147888	21.71 ± 0.09	4	20.47 ± 0.05	6	21.76 ± 0.08	13.63	0.10
HD 152590	21.37 ± 0.06	4	20.47 ± 0.07	4	21.47 ± 0.05	0.53	0.20
HD 168941	21.11 ± 0.09	3	20.10 ± 0.05	2	21.19 ^{+0.08} _{-0.07}	0.10	0.16
HD 177989	20.95 ± 0.09	3	20.12 ± 0.05	2	21.06 ± 0.07	0.07	0.23
HD 185418	21.15 ± 0.09	8	20.76 ± 0.05	5	21.41 ^{+0.06} _{-0.05}	0.87	0.45
HD 192639	21.29 ± 0.08	8	20.69 ± 0.05	5	21.47 ^{+0.06} _{-0.05}	0.86	0.33
HD 195965	20.95 ± 0.03	10	20.37 ± 0.03	2	21.13 ± 0.02	0.34	0.34
HD 202347	20.99 ± 0.10	1	20.00 ± 0.06	9	21.07 ^{+0.09} _{-0.08}	0.29	0.17
HD 203374	21.11 ± 0.09	11	20.68 ± 0.05	2	21.35 ^{+0.06} _{-0.05}	0.89	0.43
HD 206267	21.30 ± 0.15	5	20.86 ± 0.04	5	21.54 ^{+0.09} _{-0.08}	1.12	0.42
HD 207198	21.34 ± 0.17	3	20.83 ± 0.04	5	21.55 ^{+0.11} _{-0.10}	1.15	0.38
HD 207308	21.20 ± 0.10	1	20.76 ± 0.05	2	21.44 ± 0.06	...	0.42
HD 207538	21.34 ± 0.12	3	20.91 ± 0.06	5	21.58 ^{+0.08} _{-0.07}	1.40	0.43
HD 209339	21.16 ± 0.10	1	20.19 ± 0.03	2	21.24 ± 0.08	0.52	0.18
HD 210839	21.19 ± 0.06	8	20.84 ± 0.04	5	21.47 ± 0.04	1.88	0.47
HD 224151	21.32 ± 0.08	8	20.57 ± 0.05	2	21.45 ± 0.06	0.68	0.26
HD 303308	21.45 ± 0.08	3	20.23 ± 0.05	2	21.50 ± 0.07	0.39	0.11

References. — (1) Jensen & Snow (2007). (2) J. M. Shull et al., in preparation. (3) Diplas & Savage (1994). (4) Cartledge et al. (2004). (5) Rachford et al. (2002). (6) B. L. Rachford et al., in preparation. (7) Jensen et al. (2007). (8) André et al. (2003). (9) Snow et al. (2007). (10) Hoopes et al. (2003). (11) Diplas & Savage (1994), Table 2 (lines of sight with uncertain stellar parameters).

Table 4. Lines of Sight: Reddening Data

Line of Sight	E_{B-V} (mag)	Ref.	A_V (mag)	Ref.	R_V	Ref.
BD +35°4258	0.29	1	0.93	2	3.21	3
CPD -59°2603	0.46	4	1.45	3	3.15	5
HD 12323	0.24	1	0.74	2	3.08	3
HD 13745	0.46	4	1.42	2	3.09	3
HD 15137	0.31	4	1.10	2	3.55	3
HD 27778	0.37	6	1.01	3	2.73	6
HD 37021	0.54	6	2.99	3	5.54	6
HD 37061	0.52	6	2.20	3	4.23	6
HD 37903	0.35	4	1.28	3	3.66	6
HD 40893	0.46	6	1.13	3	2.46	6
HD 66788	0.20	5	0.69	2	3.45	3
HD 69106	0.18	6	0.58	2	3.22	3
HD 91597	0.27	6	1.33	2	4.93	3
HD 91651	0.30	4	0.95	2	3.17	3
HD 92554	0.39	4	1.15	2	2.95	3
HD 93205	0.37	4	1.21	2	3.27	3
HD 93222	0.37	7	1.18	2	3.19	3
HD 93843	0.34	4	1.03	2	3.03	3
HD 94493	0.20	4	0.71	2	3.55	3
HD 99857	0.33	4	1.10	2	3.33	3
HD 99890	0.24	4	0.72	2	3.00	3
HD 103779	0.21	4	0.68	2	3.24	3
HD 104705	0.26	4	0.80	2	3.08	3
HD 109399	0.26	4	0.81	2	3.12	3
HD 116781	0.34	5	1.40	2	4.12	3
HD 122879	0.36	7	1.12	2	3.11	3
HD 124314	0.53	4	1.64	2	3.09	3
HD 147888	0.47	6	1.91	3	4.06	6
HD 152590	0.46	6	1.51	3	3.28	6
HD 168941	0.37	4	1.03	2	2.78	3
HD 177989	0.25	4	0.25	2	1.00	3
HD 185418	0.50	6	1.16	3	2.32	6
HD 192639	0.66	4	1.87	3	2.83	6
HD 195965	0.25	4	0.77	2	3.08	3
HD 202347	0.19	8	0.53	2	2.79	3
HD 203374	0.60	9	1.88	2	3.13	3
HD 206267	0.53	6	1.41	3	2.66	6
HD 207198	0.62	6	1.50	3	2.42	6
HD 207308	0.52	8	1.61	2	3.10	3
HD 207538	0.64	6	1.44	3	2.25	6
HD 209339	0.38	8	1.09	2	2.87	3
HD 210839	0.57	4	1.58	3	2.77	6
HD 224151	0.44	4	1.52	2	3.45	3
HD 303308	0.45	7	1.09	2	2.42	3

References. — (1) Savage et al. (1985). (2) Neckel et al. (1980). (3) Derived from the other two quantities via the relationship $R_V \equiv A_V/E_{B-V}$. (4) Diplas & Savage (1994). (5) Jensen & Snow (2007). (6) DIB Database, <http://dib.uiuc.edu>; E_{B-V} compiled by L. M. Hobbs, R_V derived by B. L. Rachford through polarization or infrared photometry Rachford et al. (for method and examples, see 2002). (7) Aiello et al. (1988). (8) Garmany & Stencel (1992). (9) Diplas & Savage (1994), Table 2 (lines of sight with uncertain stellar parameters).

Table 5. Mg II Column Density Results

Line of Sight	$\log N(\text{Mg II})$	$\log(\text{Mg II}/\text{H})$	Mg/H (ppm)	$W_{1239.9}$	$W_{1240.4}$
BD +35°4258	$16.15^{+0.06}_{-0.08}$	$-5.15^{+0.10}_{-0.35}$	$7.1^{+1.8}_{-2.1}$	81.4 ± 10.4	54.8 ± 10.4
CPD -59°2603	16.35 ± 0.03	$-5.15^{+0.06}_{-0.08}$	$7.1^{+1.1}_{-1.3}$	112.4 ± 6.6	78.8 ± 7.4
HD 12323	$16.06^{+0.04}_{-0.05}$	$-5.23^{+0.07}_{-0.10}$	$5.9^{+1.1}_{-1.3}$	64.3 ± 5.1	43.9 ± 6.0
HD 13745	$16.18^{+0.06}_{-0.07}$	$-5.20^{+0.08}_{-0.12}$	$6.3^{+1.3}_{-1.5}$	93.3 ± 10.1	61.3 ± 10.9
HD 15137	16.15 ± 0.02	$-5.07^{+0.09}_{-0.19}$	$8.5^{+2.1}_{-3.0}$	72.1 ± 2.4	50.9 ± 2.9
HD 27778	$15.42^{+0.05}_{-0.06}$	$-5.98^{+0.07}_{-0.11}$	1.1 ± 0.2	16.0 ± 1.7	10.6 ± 1.5
HD 37021	$15.93^{+0.03}_{-0.04}$	$-5.75^{+0.10}_{-0.17}$	$1.8^{+0.5}_{-0.6}$	33.7 ± 2.2	23.7 ± 2.2
HD 37061	15.78 ± 0.03	$-5.95^{+0.08}_{-0.12}$	$1.1^{+0.2}_{-0.3}$	27.0 ± 1.5	19.8 ± 1.4
HD 37903	$15.55^{+0.07}_{-0.09}$	$-5.94^{+0.09}_{-0.12}$	1.1 ± 0.3	21.1 ± 3.1	14.2 ± 3.2
HD 40893	16.33 ± 0.03	$-5.26^{+0.07}_{-0.11}$	$5.5^{+1.0}_{-1.2}$	95.5 ± 5.0	69.8 ± 5.3
HD 66788	$16.11^{+0.08}_{-0.10}$	$-5.15^{+0.11}_{-0.17}$	$7.1^{+2.0}_{-2.3}$	81.2 ± 10.6	39.5 ± 11.1
HD 69106	$15.81^{+0.02}_{-0.03}$	$-5.30^{+0.05}_{-0.07}$	5.0 ± 0.7	37.3 ± 1.7	25.3 ± 1.8
HD 91597	16.25 ± 0.05	$-5.16^{+0.07}_{-0.09}$	$6.8^{+1.2}_{-1.3}$	94.4 ± 8.7	66.1 ± 9.6
HD 91651	$16.26^{+0.03}_{-0.04}$	$-4.90^{+0.06}_{-0.08}$	$12.7^{+1.3}_{-2.1}$	108.0 ± 6.6	72.3 ± 6.9
HD 92554	$16.37^{+0.04}_{-0.05}$	$-4.91^{+0.09}_{-0.14}$	$12.3^{+2.8}_{-3.4}$	109.4 ± 9.1	80.0 ± 9.3
HD 93205	$16.32^{+0.02}_{-0.03}$	$-5.08^{+0.05}_{-0.06}$	$8.3^{+1.0}_{-1.1}$	113.7 ± 4.9	77.9 ± 5.9
HD 93222	$16.41^{+0.01}_{-0.02}$	$-5.01^{+0.06}_{-0.07}$	$9.8^{+1.4}_{-1.7}$	114.4 ± 3.0	84.3 ± 3.6
HD 93843	16.25 ± 0.02	$-5.10^{+0.08}_{-0.10}$	$7.9^{+1.3}_{-1.6}$	104.0 ± 3.4	69.8 ± 4.1
HD 94493	16.16 ± 0.02	$-5.00^{+0.04}_{-0.05}$	9.9 ± 1.1	77.2 ± 3.2	53.5 ± 3.6
HD 99857	16.21 ± 0.03	$-5.11^{+0.06}_{-0.09}$	$7.7^{+1.2}_{-1.4}$	80.6 ± 4.1	55.8 ± 4.4
HD 99890	16.18 ± 0.03	$-4.78^{+0.10}_{-0.18}$	$16.6^{+4.2}_{-5.6}$	83.4 ± 4.5	57.3 ± 5.3
HD 103779	16.17 ± 0.02	$-5.02^{+0.08}_{-0.12}$	$9.5^{+1.9}_{-2.3}$	81.6 ± 3.4	56.0 ± 3.9
HD 104705	16.19 ± 0.02	$-4.98^{+0.06}_{-0.08}$	$10.4^{+1.4}_{-1.7}$	83.8 ± 3.2	57.2 ± 3.4
HD 109399	15.95 ± 0.05	$-5.23^{+0.07}_{-0.09}$	$5.9^{+1.0}_{-1.1}$	56.8 ± 5.0	36.9 ± 5.4
HD 116781	16.14 ± 0.03	$-5.11^{+0.08}_{-0.12}$	$7.8^{+1.5}_{-1.8}$	75.5 ± 4.4	51.8 ± 4.8
HD 122879	16.22 ± 0.02	$-5.11^{+0.08}_{-0.14}$	$7.7^{+1.6}_{-2.1}$	86.5 ± 2.8	60.4 ± 3.2
HD 124314	16.32 ± 0.02	$-5.12^{+0.07}_{-0.10}$	$7.6^{+1.3}_{-1.6}$	97.6 ± 3.0	70.9 ± 3.7
HD 147888	15.83 ± 0.03	$-5.93^{+0.07}_{-0.11}$	$1.2^{+0.2}_{-0.3}$	24.1 ± 1.5	18.9 ± 1.5
HD 152590	16.20 ± 0.03	$-5.26^{+0.05}_{-0.07}$	$5.5^{+0.7}_{-0.8}$	71.3 ± 4.3	52.1 ± 4.2
HD 168941	$15.87^{+0.08}_{-0.10}$	$-5.32^{+0.10}_{-0.14}$	$4.8^{+1.2}_{-1.3}$	42.8 ± 7.0	28.9 ± 7.0
HD 177989	15.83 ± 0.03	$-5.23^{+0.06}_{-0.09}$	$5.9^{+0.9}_{-1.1}$	40.7 ± 2.0	27.1 ± 2.2
HD 185418	15.94 ± 0.03	$-5.47^{+0.05}_{-0.07}$	$3.4^{+0.4}_{-0.5}$	41.7 ± 2.1	30.0 ± 2.1
HD 192639	16.20 ± 0.03	$-5.26^{+0.05}_{-0.07}$	$5.4^{+0.7}_{-0.8}$	60.3 ± 3.2	46.9 ± 3.7
HD 195965	$15.89^{+0.04}_{-0.05}$	-5.24 ± 0.05	5.7 ± 0.7	45.0 ± 3.4	30.3 ± 4.1
HD 202347	$15.62^{+0.04}_{-0.05}$	$-5.45^{+0.08}_{-0.12}$	$3.5^{+0.7}_{-0.8}$	27.5 ± 2.2	17.6 ± 2.2
HD 203374	16.07 ± 0.02	$-5.28^{+0.05}_{-0.07}$	$5.3^{+0.7}_{-0.8}$	63.3 ± 2.7	44.3 ± 2.8
HD 206267	16.05 ± 0.04	$-5.48^{+0.08}_{-0.13}$	$3.3^{+0.6}_{-0.9}$	58.1 ± 4.2	40.7 ± 4.7
HD 207198	16.08 ± 0.02	$-5.47^{+0.08}_{-0.16}$	$3.4^{+0.7}_{-1.0}$	56.6 ± 2.2	40.8 ± 2.7
HD 207308	15.93 ± 0.05	$-5.51^{+0.07}_{-0.10}$	$3.1^{+0.5}_{-0.6}$	45.9 ± 4.1	31.7 ± 4.6
HD 207538	$16.07^{+0.03}_{-0.04}$	$-5.51^{+0.07}_{-0.10}$	$3.1^{+0.5}_{-0.6}$	58.2 ± 3.5	41.4 ± 4.1
HD 209339	16.04 ± 0.02	$-5.21^{+0.07}_{-0.11}$	$6.2^{+1.1}_{-1.3}$	53.9 ± 1.8	38.4 ± 2.0
HD 210839	16.05 ± 0.03	$-5.42^{+0.04}_{-0.05}$	3.8 ± 0.4	63.1 ± 3.3	42.9 ± 3.7
HD 224151	16.30 ± 0.03	$-5.15^{+0.06}_{-0.08}$	$7.1^{+1.0}_{-1.2}$	104.6 ± 5.8	72.4 ± 6.5
HD 303308	$16.34^{+0.04}_{-0.05}$	$-5.15^{+0.07}_{-0.10}$	$7.0^{+1.3}_{-1.4}$	108.1 ± 8.6	75.8 ± 9.0

Table 6. Comparison with CLMS

Line of Sight	log $N(\text{Mg II})$			
	This paper	CLMS AOD ^a	CLMS PF ^b	CLMS AE ^c
HD 12323	$16.06^{+0.04}_{-0.05}$	16.03 ± 0.02	16.04 ± 0.05	0.05
HD 27778	$15.42^{+0.05}_{-0.06}$	15.49 ± 0.02	15.48 ± 0.01	0.02
HD 37021	$15.93^{+0.03}_{-0.04}$	15.85 ± 0.02	15.90 ± 0.02	0.03
HD 37061	15.78 ± 0.03	15.78 ± 0.01	15.80 ± 0.05	0.05
HD 37903	$15.55^{+0.07}_{-0.09}$	15.65 ± 0.02	15.62 ± 0.06	0.06
HD 122879	16.22 ± 0.02	16.22 ± 0.02	16.23 ± 0.01	0.02
HD 147888	15.83 ± 0.03	15.84 ± 0.03	16.03 ± 0.03	0.04
HD 152590	16.20 ± 0.03	16.19 ± 0.02	16.20 ± 0.09	0.09
HD 185418	15.94 ± 0.03	15.97 ± 0.02	15.96 ± 0.01	0.02
HD 192639	16.20 ± 0.03	16.19 ± 0.02	16.21 ± 0.02	0.03
HD 207198	16.08 ± 0.02	16.08 ± 0.01	16.08 ± 0.02	0.02

^aCLMS results, apparent optical depth method (uncorrected).

^bCLMS results, profile fitting method.

^cAdopted error of CLMS. Note that CLMS adopt profile fitting results for the best column density, but adopt errors that are the errors of the apparent optical depth and profile fitting methods added in quadrature.

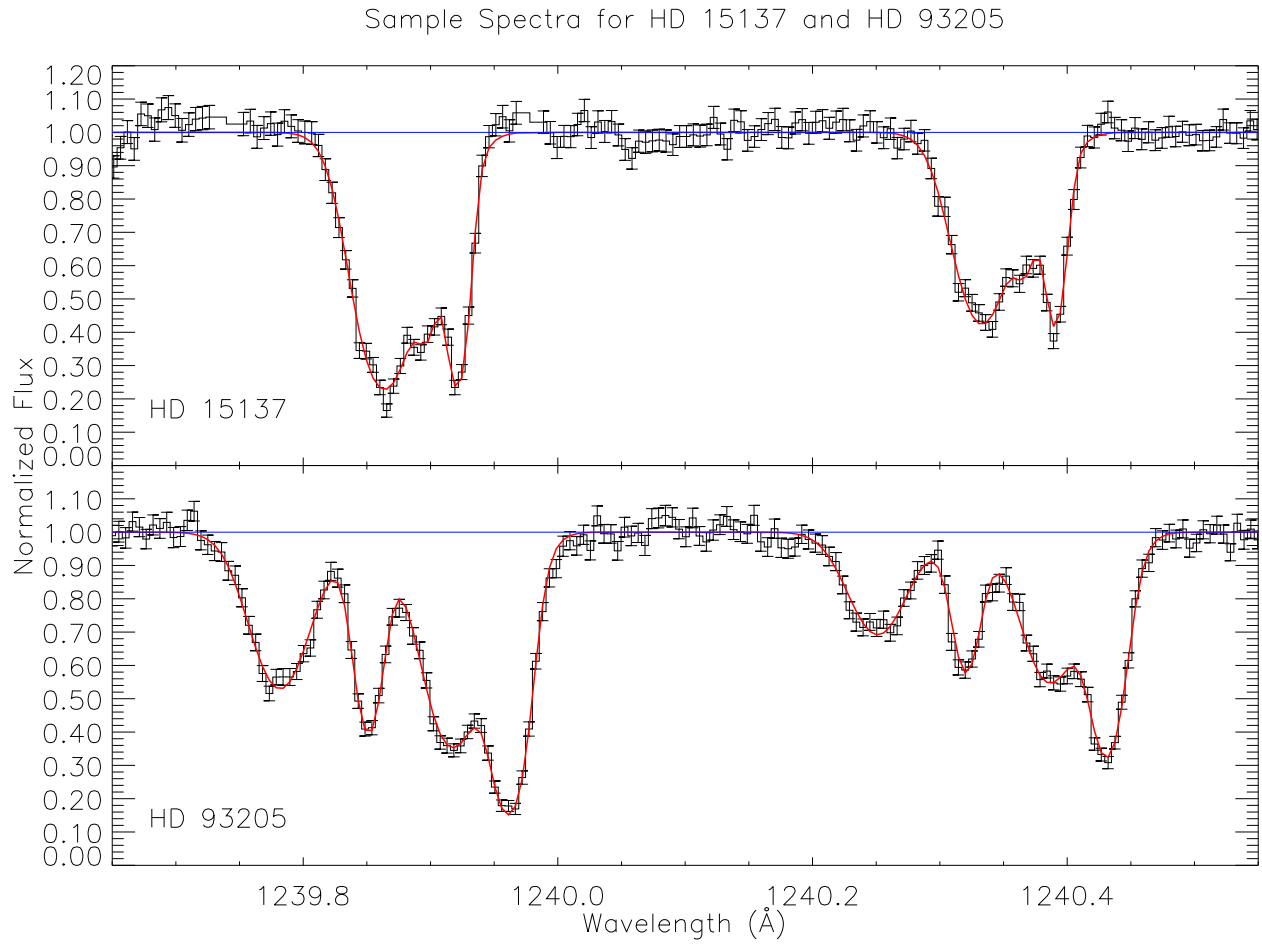


Fig. 1.— Two samples of the fits made by our techniques. Spectra are shown normalized but without velocity correction. Error bars for the STIS data are shown, with profile fits plotted in red and the continuum level plotted in blue. **Top:**—HD 15137. **Bottom:**—HD 93205.

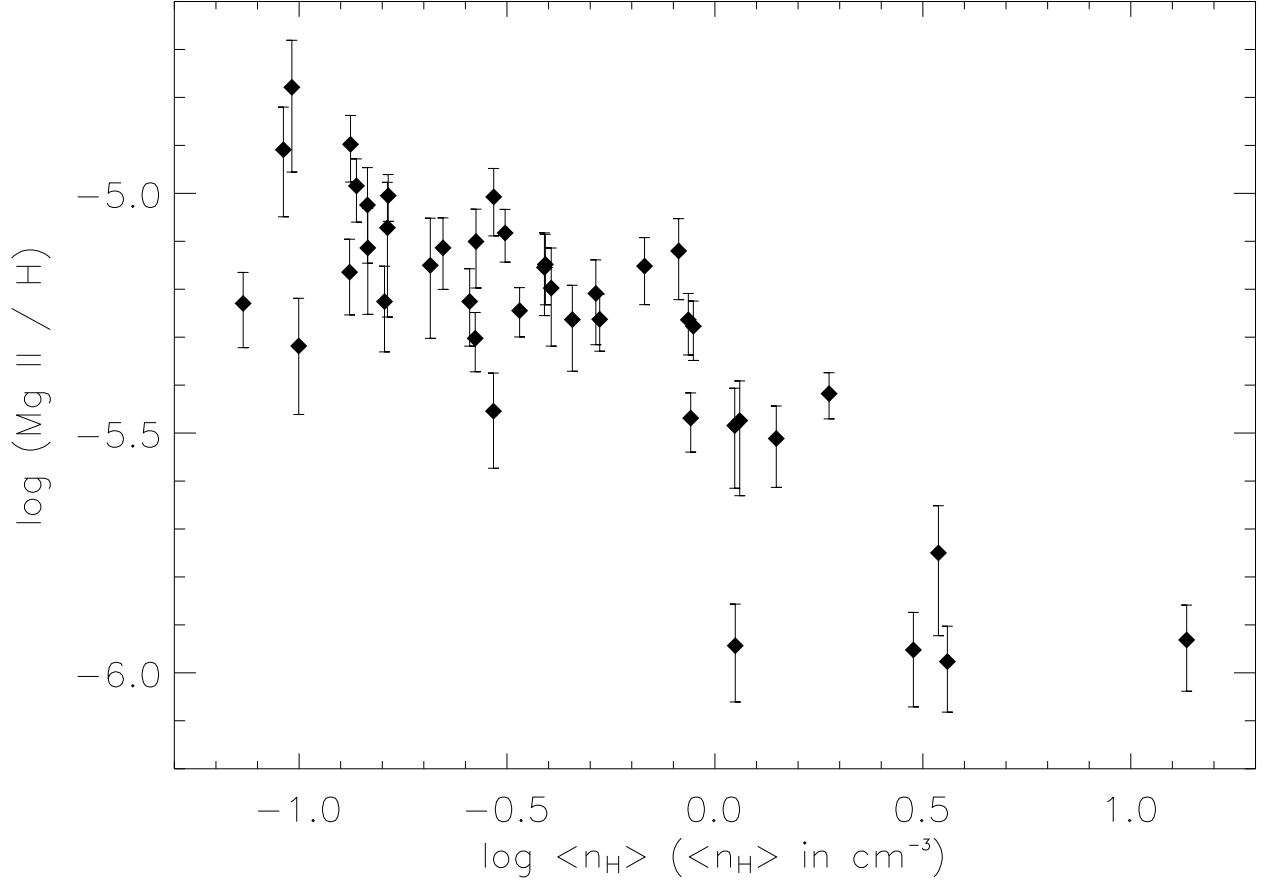


Fig. 2.— The logarithmic abundance of Mg II relative to hydrogen plotted against the logarithm of the total volume density of hydrogen. The five lines of sight with the greatest magnesium depletion are (in order of decreasing depletion) HD 27778, HD 37061, HD 37903, HD 147888, and HD 37021. The Mg II / H_{tot} ratio and $\langle n_{\text{H}} \rangle$ for HD 37021 and HD 37061 are based only on atomic hydrogen, due to a lack of data on H_2 .

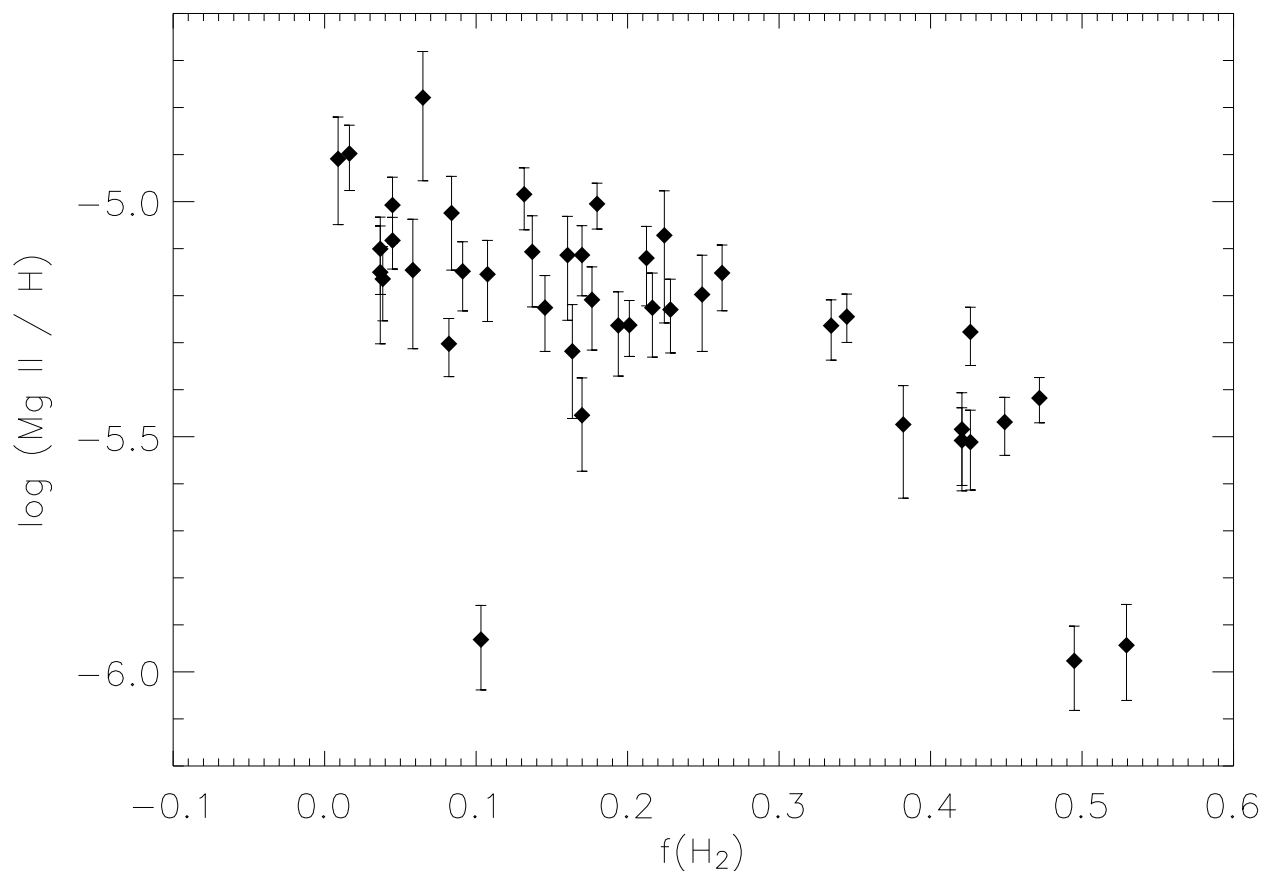


Fig. 3.— The logarithmic abundance of Mg II relative to hydrogen plotted against the molecular fraction of hydrogen. Two lines of sight with large depletions are not plotted due to a lack of information on H_2 , HD 37021 and HD 37061. The anomalous point, with a large depletion but small $f(\text{H}_2)$, is the HD 147888 line of sight. Compare this figure to the upper right panel of Figure 9 of CLMS. See §3.1.1 in this paper for further discussion.

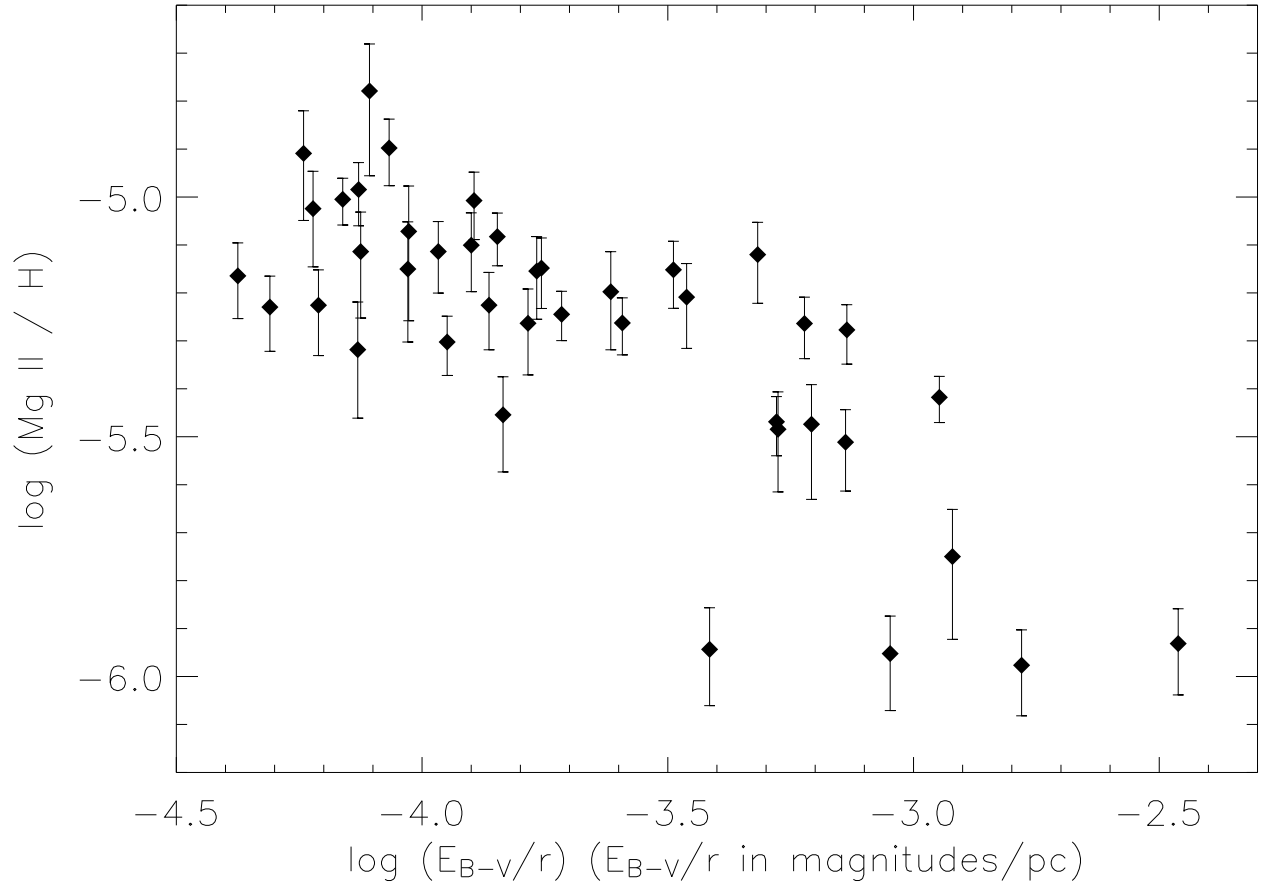


Fig. 4.— The logarithmic abundance of Mg II relative to hydrogen plotted against the logarithm of selective extinction divided by pathlength. See §3.1.2 for further discussion.

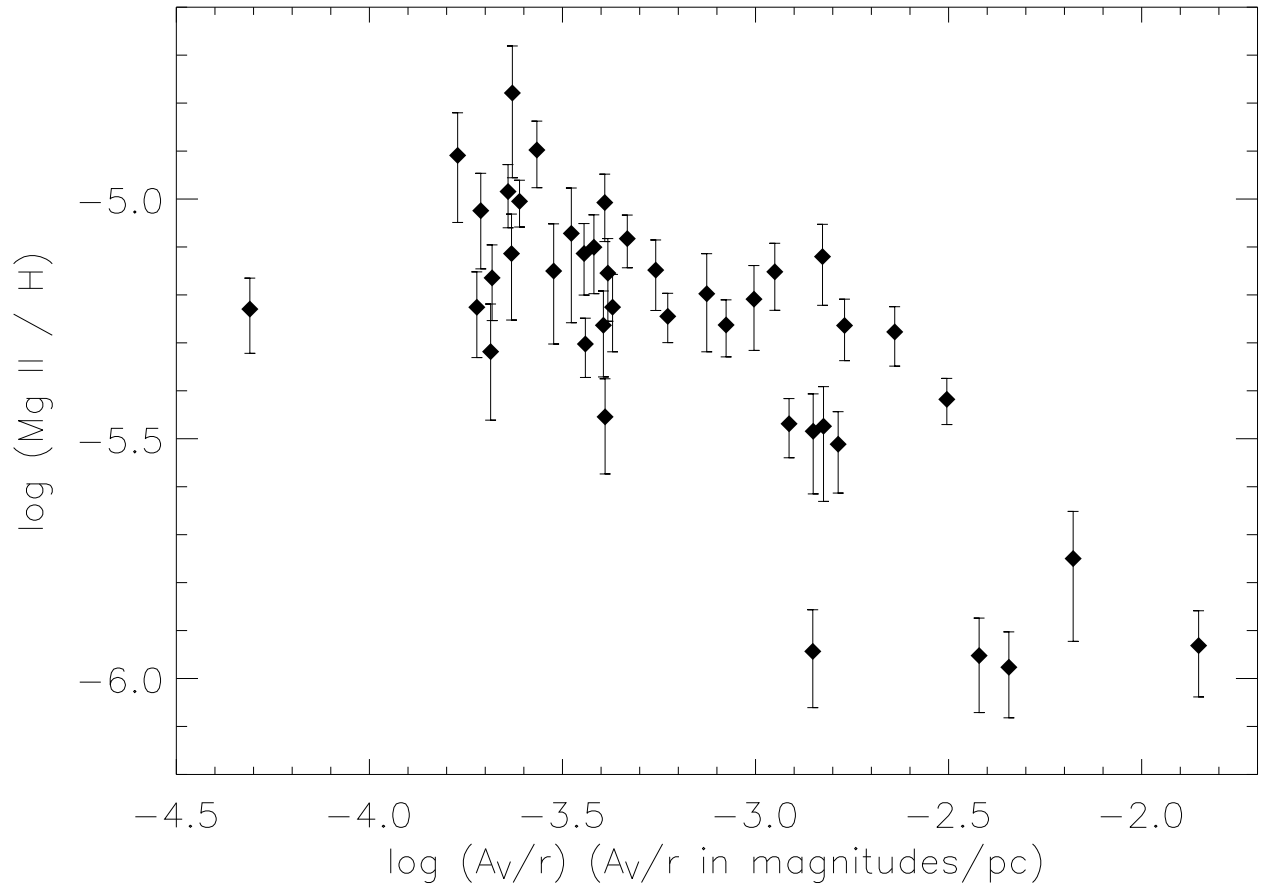
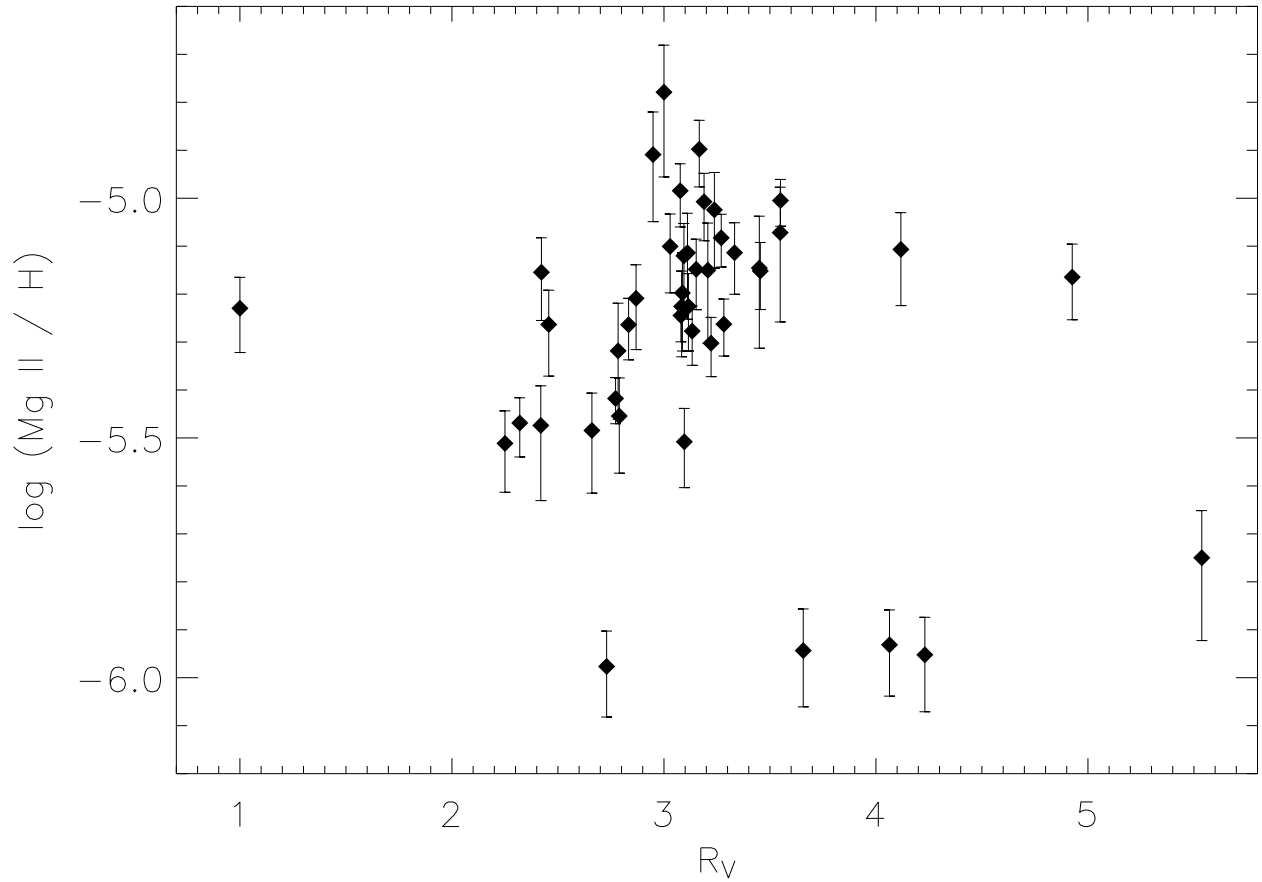


Fig. 5.— The logarithmic abundance of Mg II relative to hydrogen plotted against the logarithm of total visual extinction divided by pathlength. See §3.1.2 for further discussion.



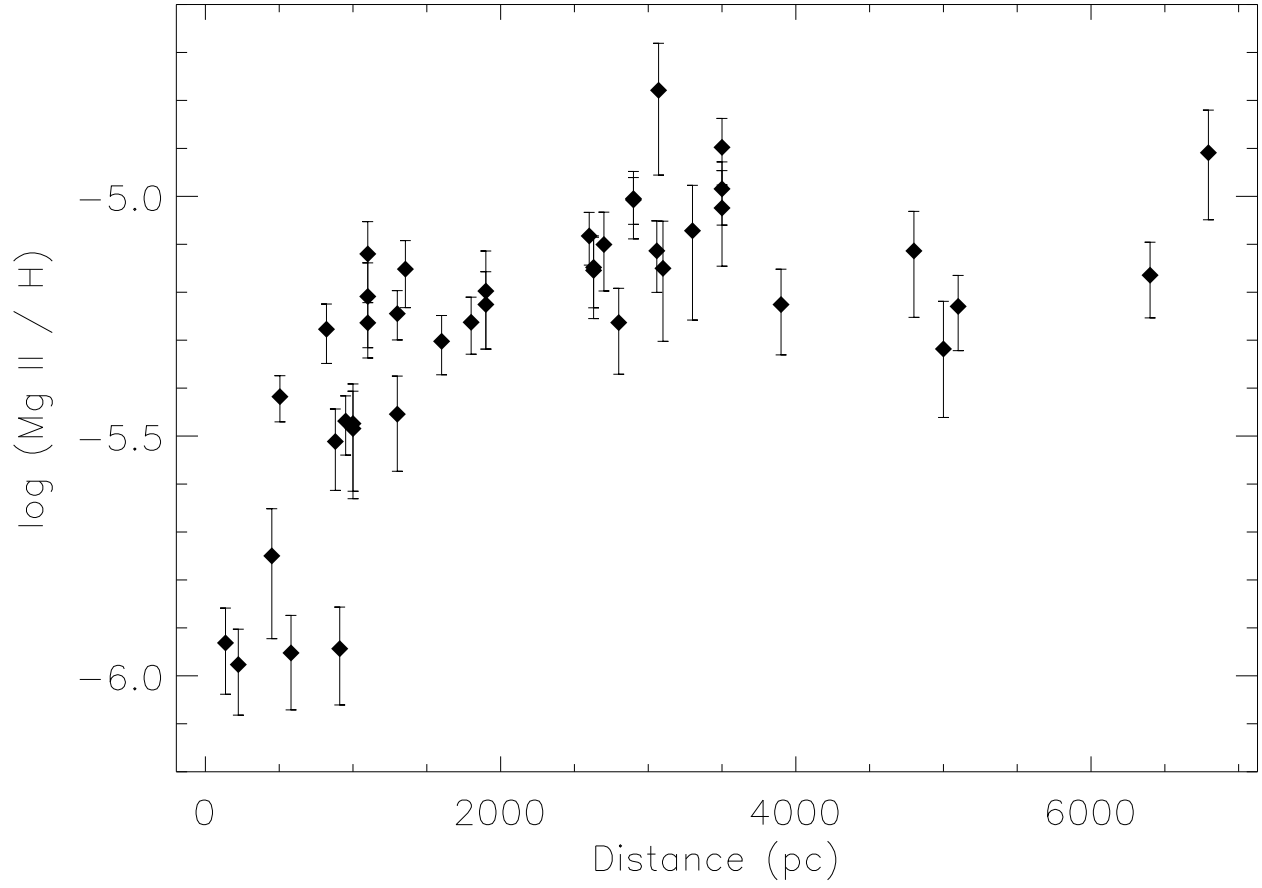


Fig. 7.— The logarithmic abundance of Mg II relative to hydrogen plotted against path-length. Note the trend of decreasing depletion up to about 1.5–2 kpc, and relatively constant depletion beyond 2 kpc.